


Manipulating thermal light via displaced-photon subtraction

G. Tatsi¹, D. W. Canning^{2,*}, U. Zanforlin^{2,*}, L. Mazzarella^{1,†}, J. Jeffers¹ and G. S. Buller²
¹*Scottish Universities Physics Alliance, Department of Physics, University of Strathclyde, John Anderson Building, 107 Rottenrow, Glasgow G4 0NG, United Kingdom*

²*Scottish Universities Physics Alliance, Institute of Photonics and Quantum Sciences, School of Engineering and Physical Sciences, Heriot-Watt University, David Brewster Building, Edinburgh EH14 4AS, United Kingdom*

 (Received 24 November 2020; revised 12 November 2021; accepted 11 April 2022; published 2 May 2022)

Thermal radiation played a pivotal role in the preliminary development of quantum physics where it helped resolve the apparent incongruity of the ultraviolet catastrophe. In contemporary physics, thermal state generation and manipulation finds new application in fields such as quantum imaging and quantum illumination and as a practical realization of Maxwell’s demon. These applications often go hand in hand with photon subtraction operations which probabilistically amplify the mean photon number (MPN) of thermal light as a result of its super-Poissonian photon statistics. In this article, we introduce an operation for thermal states of light based on a generalized photon subtraction scheme. *Displaced-photon subtraction* (DPS) makes use of coherent state displacement followed by a subsequent anti-displacement in combination with single-photon detection to probe the MPN of a thermal state. We find regimes in which the output of a successful DPS is amplified, unchanged, or attenuated relative to the unconditioned output state. The regime of operation is controlled via the magnitude of the coherent displacement. A theoretical description of generalized photon subtraction of a displaced thermal state is derived via a two-mode moment-generating function (MGF) and used to describe generalized DPS. We perform a proof of principle experimental implementation of DPS for the case of a balanced beam splitter for which results demonstrate good agreement with the model.

DOI: [10.1103/PhysRevA.105.053701](https://doi.org/10.1103/PhysRevA.105.053701)

I. INTRODUCTION

The historical significance of thermal light in quantum optics is without question: Planck argued the quantization of light from black-body radiation, and Hanbury-Brown and Twiss (HBT) first investigated photon statistics in astronomical sources [1,2]. Contemporary experiments combining thermal light and photon subtraction techniques have implemented effects such as ghost imaging [3–5], quantum illumination [6], and the “quantum” vampire effect [7,8], as well as tests of fundamental physics such as the bosonic commutation relation [9,10] and Maxwell’s demon [11]. While much attention has been paid to photon-subtracted thermal states [12–21], comparatively little has been paid to photon-subtracted displaced thermal states [22]. Such states arise in quantum state discrimination tasks [23,24] where a binary coherent state signal, $|\pm\alpha\rangle$, has been corrupted by thermal

noise [25,26] corresponding, for example, to ambient light in free space [27] or Raman scattering in optical fiber [28].

In this article, we demonstrate, both theoretically and experimentally, a quantum optical operation on a thermal state, which we call displaced-photon subtraction (DPS). We derive a two-mode moment-generating function (MGF) that fully describes the photon statistics of the output of a beam splitter given an arbitrarily displaced thermal state on one input and a coherent state of arbitrary complex amplitude on the other. We use the MGF to investigate the effect of photon subtraction on a displaced thermal state before introducing the new operation. We observe that thermal state displacement followed by antidisplacement at a beam splitter affects the mean photon number (MPN) of the output thermal state depending on the magnitude of the displacement itself.

II. PHOTON SUBTRACTION

Photon subtraction is the process by which the presence of a single photon is destructively measured in a mode of the electromagnetic field. It is a mature and versatile technique used in applications such as coherent state amplification [29–34] and nonclassical state generation [35–38]. It transforms an input state, $\hat{\rho}$, to an output state, $\hat{\rho}_{-1}$,

$$\hat{\rho}_{-1} = \frac{\hat{a}\hat{\rho}\hat{a}^\dagger}{\text{Tr}[\hat{\rho}\hat{a}^\dagger\hat{a}]}, \quad (1)$$

where \hat{a} (\hat{a}^\dagger) is the bosonic annihilation (creation) operator of the mode. At low optical powers, it can be approximated

*These authors contributed equally to the experimental aspects of this work.

†Present address: Quantum Sciences and Technology Group, Jet Propulsion Laboratory, California Institute of Technology, 4800 Oak Grove Drive, Pasadena, CA 91109, USA.

Published by the American Physical Society under the terms of the [Creative Commons Attribution 4.0 International license](https://creativecommons.org/licenses/by/4.0/). Further distribution of this work must maintain attribution to the author(s) and the published article’s title, journal citation, and DOI.

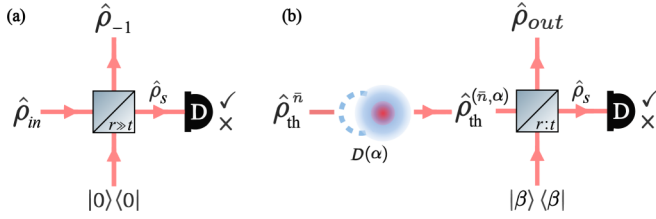


FIG. 1. (a) Photon subtraction occurs when the detector, D, registers a click, \checkmark . (b) Generalized two-mode scheme used to investigate the photon statistics of displaced thermal states, and displaced photon subtraction of thermal states.

experimentally with a highly reflective beam splitter and a single-photon detector, D, operating in Geiger mode, as shown in Fig. 1(a). The photon subtracted state is obtained by conditioning the output (reflected relative to the input) on a detection event, or *click*, at D. Despite its name, photon subtraction is capable of increasing, leaving unchanged, or decreasing the MPN of the output state, $\langle\hat{n}\rangle_{-1}$, depending on whether the input exhibits super-Poissonian, Poissonian, or sub-Poissonian statistics respectively [39]. More formally,

$$\langle\hat{n}\rangle_{-1} = \frac{\text{Tr}[\hat{\rho}\hat{a}^{\dagger 2}\hat{a}^2]}{\text{Tr}[\hat{\rho}\hat{a}^{\dagger}\hat{a}]} = g^{(2)}(0)\langle\hat{n}\rangle, \quad (2)$$

having defined $\langle\hat{n}\rangle = \text{Tr}[\hat{\rho}\hat{a}^{\dagger}\hat{a}]$ as the MPN, and $g^{(2)}(0) = \text{Tr}[\hat{\rho}\hat{a}^{\dagger 2}\hat{a}^2]/(\text{Tr}[\hat{\rho}\hat{a}^{\dagger}\hat{a}])^2$ as the second-order correlation function at zero delay time, of the input state, $\hat{\rho}$. Thermal states show super-Poissonian photon statistics and have $g^{(2)}(0) = 2$, meaning that their MPN is boosted by a successful photon subtraction. Vidrighin *et al.* recently harnessed this somewhat counterintuitive effect to extract work in a photonic implementation of Maxwell's demon [11].

III. MOMENT-GENERATING FUNCTION

A convenient tool for parametrizing photon statistics is the MGF, recently advocated by Bogdanov *et al.* and Barnett *et al.* [39,40], defined as

$$M(\mu) = \text{Tr}[\hat{\rho} : e^{-\mu\hat{a}^{\dagger}\hat{a}} :], \quad (3)$$

where $::$ denotes normal ordering. Equation (3) can then be combined with the Kelley-Kleiner formula [41] to express the probability of a detection event as $P_{\checkmark} = 1 - M(\eta)$, where η is the quantum efficiency of the detector. The definition of the

$$M(\mu_1, \mu_2) = \frac{1}{1 + \mu_1 t^2 \bar{n} + \mu_2 r^2 \bar{n}} \exp - \frac{\mu_1 |t\alpha - r\beta|^2 + \mu_2 |r\alpha + t\beta|^2 + |\beta|^2 \bar{n} \mu_1 \mu_2}{1 + t^2 \mu_1 \bar{n} + r^2 \mu_2 \bar{n}}. \quad (11)$$

The single-mode MGF for the unconditioned output, $\hat{\rho}_{out}$, follows immediately since $M(\mu_1, 0) = M_1(\mu_1)$, and the corresponding MPN via Eq. (7) is

$$\langle\hat{n}\rangle = \bar{n}r^2 + |r\alpha + t\beta|^2. \quad (12)$$

MGF can be extended to two modes:

$$M(\mu_1, \mu_2) = \text{Tr}_{1,2}[\hat{\rho}_{12} : e^{-\mu_1 \hat{a}_1^{\dagger} \hat{a}_1 - \mu_2 \hat{a}_2^{\dagger} \hat{a}_2} :], \quad (4)$$

from which we can recover the respective single-mode MGFs by setting the other mode's parameter to 0, resulting in the the second mode being traced out.

If a Geiger mode detector monitors the first mode, the MGF of the second mode, conditioned on the absence of a click event from the first mode, is [42]

$$M_{\mathcal{X}}(\mu_2) = \frac{M(\eta, \mu_2)}{M(\eta, 0)}, \quad (5)$$

and when conditioned on a click event,

$$M_{\checkmark}(\mu_2) = \frac{M(0, \mu_2) - M(\eta, \mu_2)}{M(0, 0) - M(\eta, 0)}. \quad (6)$$

The utility of MGFs for the investigation of photon statistics is apparent when we consider that the factorial moments are obtained from the MGF via

$$\langle\hat{n}^{(m)}\rangle = \left| \left(-\frac{d}{d\mu} \right)^m M(\mu) \right|_{\mu=0} \quad (7)$$

from which MPN of the state straightforwardly follows as $\langle\hat{n}\rangle = -M'(\mu)|_{\mu=0}$ with $M'(\mu) = dM(\mu)/d\mu$.

A quantum optical state, $\hat{\rho}$, is sometimes expressed in the coherent state basis via the Glauber-Sudarshan P representation [1],

$$\hat{\rho} = \int P(\gamma) |\gamma\rangle\langle\gamma| d^2\gamma, \quad (8)$$

where the integral is understood to be over the complex plane, $d^2\gamma = d\text{Re}\gamma d\text{Im}\gamma$, and the P function, $P(\gamma)$, represents a true probability distribution for so-called *classical* states of light, i.e., those that can be parameterized analogously to a monochromatic electromagnetic wave [43,44]. In particular, a displaced thermal state has the following P function,

$$P(\gamma) = \frac{1}{\pi\bar{n}} \exp -\frac{|\gamma - \alpha|^2}{\bar{n}}, \quad (9)$$

from which the MGF can be expressed in integral form as

$$M(\mu) = \int P(\gamma) \exp -\mu|\gamma|^2 d^2\gamma. \quad (10)$$

In order to investigate the photon statistics of displaced thermal light, we consider a thermalized input, of thermal MPN, \bar{n} , displaced by a complex amplitude α , and mixed with a coherent state, $|\beta\rangle$ at a generic beam splitter ($t:r$). This generalized photon subtraction scheme is depicted in Fig. 1(b) and gives rise to the following two-mode MGF for the output of the beam splitter

Similarly, from Eqs. (5) and (6) respectively, the output MPN conditioned on no click, \mathcal{X} , and on a click, \checkmark , are

$$\langle\hat{n}\rangle_{\mathcal{X}} = \frac{\bar{n}r^2(1 + \bar{n}t^2\eta) + |t\beta(1 + \eta\bar{n}) + r\alpha|^2}{(1 + \bar{n}t^2\eta)^2} \quad (13)$$

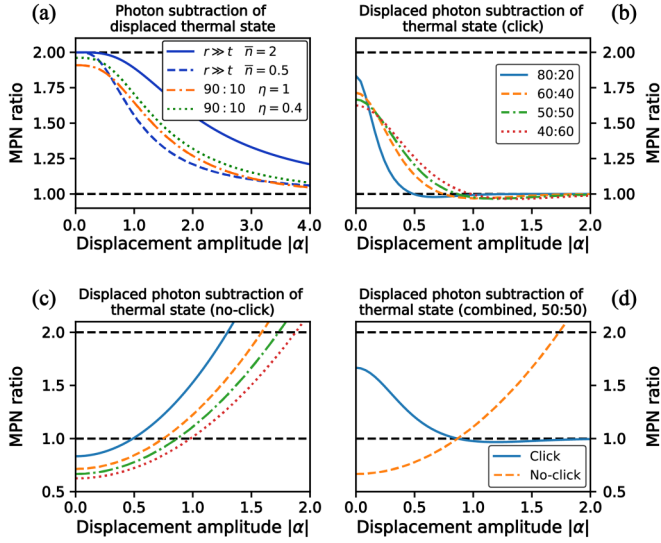


FIG. 2. (a) MPN ratio of successful to unconditioned output of photon subtraction of a displaced thermal state; [(b), (c)] MPN ratio of successful (unsuccessful) to unconditioned output of displaced photon subtraction of a thermal state, and (d) combined plot of the 50 : 50 BS case, all as a function of displacement amplitude, $|\alpha|$.

and

$$\langle \hat{n} \rangle_{\checkmark} = \frac{\langle \hat{n} \rangle - P_{\checkmark} \langle \hat{n} \rangle_{\times}}{P_{\checkmark}}, \quad (14)$$

respectively, where we have defined $P_{\checkmark} = 1 - P_{\times}$ where

$$P_{\times} = \frac{1}{1 + \bar{n}t^2\eta} \exp - \frac{\eta|t\alpha - r\beta|^2}{1 + \bar{n}t^2\eta}. \quad (15)$$

IV. PHOTON SUBTRACTION OF A DISPLACED THERMAL STATE

By comparing Figs. 1(a) and 1(b), it is clear that the MGF of a photon subtracted displaced thermal state can be calculated by setting $\beta = 0$ in the limit $r^2 \rightarrow 1$, and using Eq. (6) to condition on a click. This results in the following single-mode MGF:

$$M_{\text{th}}^{\alpha}(\mu)_{-1} = \frac{|\alpha|^2 + \bar{n} + \bar{n}^2\mu}{(\bar{n} + |\alpha|^2)(1 + \bar{n}\mu)^3} \exp - \frac{\mu|\alpha|^2}{1 + \bar{n}\mu}. \quad (16)$$

The MPN of the photon subtracted state is then calculated via Eq. (7) to be

$$\langle \hat{n} \rangle_{\text{th}_{-1}}^{\alpha} = \frac{|\alpha|^4 + 4|\alpha|^2\bar{n} + 2\bar{n}^2}{|\alpha|^2 + \bar{n}}. \quad (17)$$

The ratio of the MPN of the photon-subtracted displaced thermal state to that of the unconditioned output state is shown in Fig. 2(a) for true photon subtraction ($r^2 \rightarrow 1$) and for a typical experimental implementation ($r^2 = 0.9$). The behavior at the two extremes is as expected: When there is no displacement ($\alpha = 0$), the input state is a thermal state and photon subtraction maximally boosts the MPN ratio (twofold in the case of true photon subtraction); as the displacement increases, the boost is less pronounced as the thermal part becomes less significant before finally, at large displacements, approaching unity as the thermal noise contribution to the

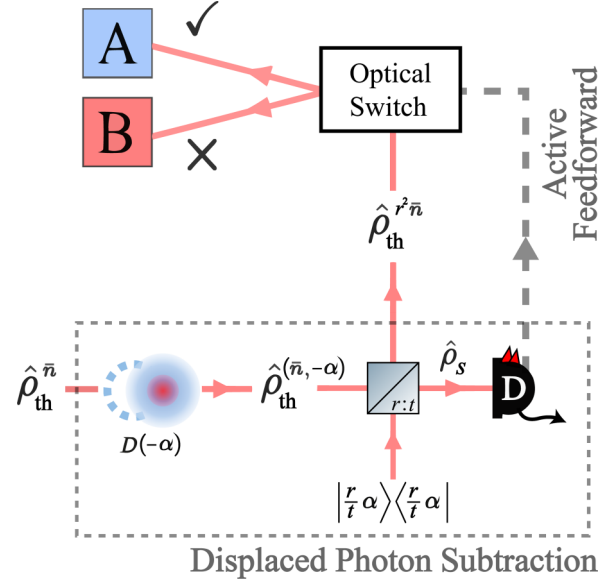


FIG. 3. Schematic of the displaced-photon subtraction operation with a proposed implementation of a photonic Maxwell's demon. Based on the result of the photodetection at D , the demon decides which reservoir to deposit the light into via an active feedforward. This could be performed with a polarization modulator combined with a polarizing beam splitter, or directly with an acousto-optic modulator.

state becomes negligible and the state behaves like a coherent state. Comparing different thermal MPNs, one can also see that as the input state is less “noisy,” the more quickly it approaches Poissonian statistics. The utility of the generalized two-mode approach is shown by plotting the same ratio for a realistic experimental implementation of photon subtraction with a 90 : 10 beam splitter (BS) for a theoretically perfect detector $\eta = 1$, and for a less efficient detector $\eta = 0.4$ typical of a thick-junction silicon-based single-photon avalanche diode (Si-SPAD) at ≈ 850 nm [45]. Interestingly, at low displacements the imperfect detector will clearly suppress the success rate of photon subtraction; however, the effect itself is not diminished but is greater than it would be for a perfect detector. This is because a click on a poor efficiency Geiger mode detector corresponds to a collapse onto a mixed state with a higher MPN compared to the one on a perfect detector. As the efficiency drops, the MPN of the collapsed state increases. It is important to mention that all these effects are independent of the type of single-photon detector used as conditioning criterion, e.g., SPAD or photon number resolving detector, since the probability of detecting multiple photons is almost negligible, and hence there is little advantage in knowing that a successful detection event was triggered by more than one photon.

V. DISPLACED PHOTON SUBTRACTION OF A THERMAL STATE

Motivated by the behavior of displaced thermal states when subjected to a photon subtraction, we considered what we will refer to as a *displaced-photon subtraction* (DPS) acting on a thermal state (see dashed box in Fig. 3). In this scheme,

the input is displaced by some amplitude, say $-\alpha$ (without loss of generality), before being mixed with a coherent state of displacement $|(r/t)\alpha$ at the beam splitter. Choosing real reflectivity and transmissivity, one can think of the BS as imparting a π phase change on reflection into the detector mode and no phase change on reflection into the output mode, resulting in the coherent part of the two inputs interfering constructively in the detector mode and destructively in the output mode. This is consistent with Eq. (12) where it is clear that the output MPN of DPS is constant for all α . Thus, DPS takes a thermal state as input and outputs a thermal state attenuated by r^2 irrespective of the value of α . It is important to stress that the ability of the displacement stage to route coherent light only to one of the two output modes of the BS is guaranteed only when the relative phase difference between the two input states is actively monitored and kept constant. In our case, this was possible due to an active stabilization feedback mechanism implemented during the entire data acquisition process (see Appendix B for more details). However, when we plot how the output is affected by conditioning on detector events, we see that the amplitude plays an interesting role in the photon statistics. Figure 2(b) shows the ratio $\langle \hat{n} \rangle_{\checkmark} / \langle \hat{n} \rangle$ of the output of DPS for various BS ratios. Figure 2(c) plots the equivalent ratio, $\langle \hat{n} \rangle_{\times} / \langle \hat{n} \rangle$, for the absence of a click.

It is instructive to consider the 50 : 50 case [shown combined for both conditions in Fig. 2(d)] as, when $\alpha = 0$, the scheme reduces to a HBT interferometer [2] and the results are as expected: When conditioned on (the absence of) a detection event, the MPN is boosted (suppressed). As we increase the displacement, we leave the thermal output completely unchanged, while routing all of the coherent light to the detector. The MPN boosting effect persists at low displacements where the thermal part dominates in the detector mode. Conversely, at high displacements, the coherent part of the light on the detector arm dominates and the correlation induced by the thermal part of the output is completely masked. However, for an intermediate range of displacements, the addition of coherent light to the detector arm causes a suppression where the MPN photon number of the output is “cooled” when DPS has been successful. This might seem surprising at first sight, but one needs to keep in mind that the output state after a successful DPS is a non-Gaussian state, as attested by its non-Gaussian P function [see Eq. (E1) of Appendix E].

VI. EXPERIMENTAL VERIFICATION

Figure 4 shows the schematic representation of the interferometric setup used for our proof of principle experimental demonstration of DPS (see Fig. 6 for the explicit optical setup). A single-mode coherent state, $|2\alpha\rangle$, and a local oscillator (LO) are derived from a vertical cavity surface-emitting laser (VCSEL) diode (842.2 nm central wavelength, 0.11 nm FWHM linewidth, 200 kHz effective repetition rate). The coherent state is fed into a loss balanced Mach-Zehnder interferometer (MZI) with an auxiliary balanced BS inserted into the upper arm. The free input mode of the auxiliary BS is fed with a thermal state derived from the LO using two commercial electro-optic modulators (EOMs) driven with paired pulse-patterns ($V_{|\gamma|}, V_{\phi}$) from a dual-output arbitrary wave-form generator (AWG) with voltages chosen to im-

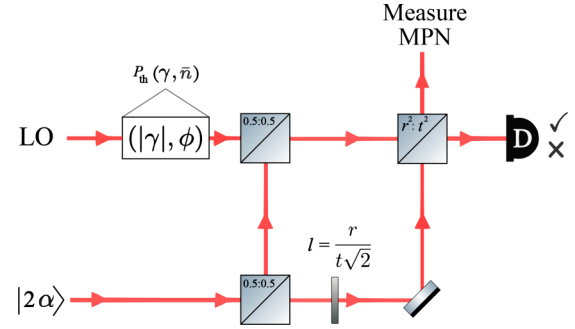


FIG. 4. Interferometric implementation of displaced photon subtraction implementable with a single coherent source. The scheme consists of a loss-balanced Mach-Zehnder interferometer (MZI) with added thermal noise derived from a local oscillator (LO) on one arm.

part amplitude and phase changes according to the thermal state P function, Eq. (9), for $\bar{n} = 0.5, 1, 2$, and zero displacement [30]. Part of the LO field was also used to perform a full tomographic reconstruction of the displaced output state (not shown—see Appendix B for a detailed description). With the coherent input blocked ($\alpha = 0$), the thermal MPNs were experimentally measured at the tomography stage to be $\bar{n} = 2.028, 1.006, 0.522 (\pm 0.008)$ and average $g^{(2)}(0) = 1.873 \pm 0.002$. As opposed to an *Arecchi's wheel* style setup [46], this has future potential to be implemented in a fully integrated-photonic platform as it requires only BSs, phase modulation, and random number generation [34,47,48]. Commercial thick-junction silicon SPADs ($\eta \approx 40\%$ for NIRW) were used to detect the different states and allowing to resolve single-photon correlations with picosecond resolution using a dedicated time-correlated single-photon counting module. The interferometers were implemented using commercially available fiber-coupled polarization-maintaining components

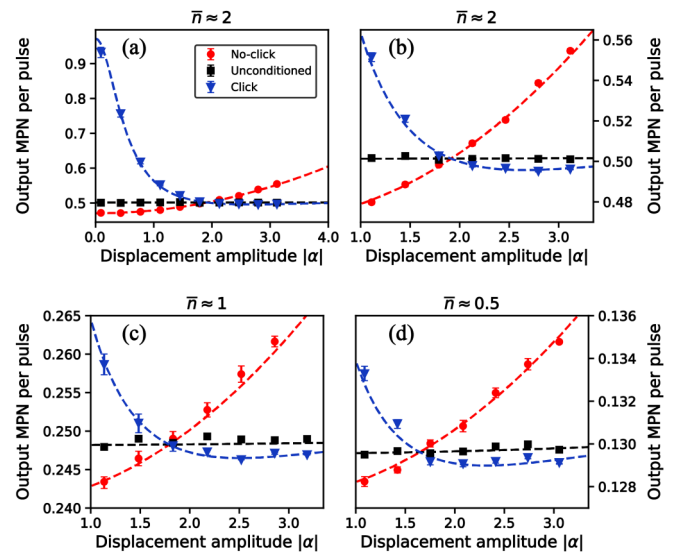


FIG. 5. [(a)–(d)] Theoretical (dashed) and experimental (markers) plots of displaced photon subtraction at a balanced beam splitter for different values of \bar{n} . (a) Full range of measurements for $\bar{n} \approx 2$. [(b)–(d)] Measurements enlarged on crossover point for $\bar{n} \approx 2, 1, 0.5$ respectively.

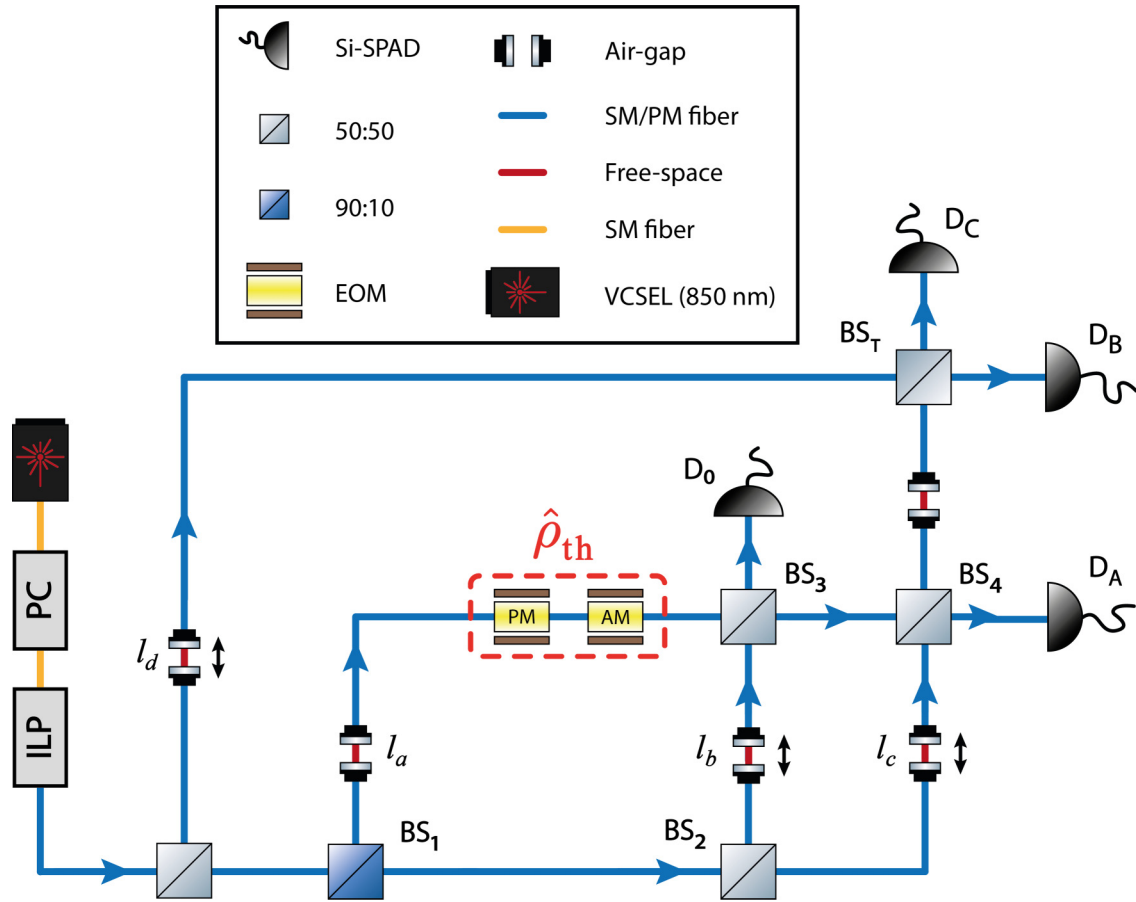


FIG. 6. Optical setup of displaced photon subtraction of a displaced thermal state system. VCSEL, vertical-cavity surface-emitting laser diode. EOM, electro-optic modulator. PC, polarization controller. ILP, in-line fiber polarizer. Si-SPAD, silicon single-photon avalanche diode. BS, beam splitter. SM fiber, single-mode fiber. SM/PM fiber, single-mode polarization maintaining fiber.

allowing both thermal and mechanical stability throughout the data acquisitions. We measured the MPN of the output thermal state for a range of α values and \bar{n} values plotting the data points in Fig. 5 compensating for imperfect interferometric visibility and optical loss. Magnifying the plots around the region of interest [Figs. 5(b)–5(d)] clearly shows the three regimes of the conditioned output. Figure 8 reports the full range of experimentally measured values for $\bar{n} \approx 1$ and 0.5.

VII. DISCUSSION

In this article, we introduced a generic two-mode MGF which showed how it can be used to generalize a photon-subtraction measurement. We first used it to describe the effect of experimental photon subtraction on the photon statistics of displaced thermal states before introducing a new technique, *displaced-photon subtraction* and the effect it has on the MPN of its output. We showed that it can mimic photon subtraction on all categories—sub-Poissonian, Poissonian, and super-Poissonian—of light, depending on the displacement, the MPN can be increased, decreased, or preserved compared to the unconditioned output (albeit while attenuating the state). We expect that the two-mode MGF will certainly find use in future theoretical and experimental studies of displaced thermal light.

We envision three areas of research making use of the DPS scheme. First, the scheme could be used in photonic Maxwell’s demon experiment [11], where the demon can choose the displacement amplitude, record the detection result, and deposit each pulse in an appropriate “cool” or “warm” reservoir depending on the detection result using an active feedforward scheme [49,50], as illustrated in Fig. 3. Second, in future development we would investigate the scheme’s use as state generator, or eavesdropper, in a central broadcasting quantum communications protocol based on thermal light [51–54]. Lastly, the tomography stage could be upgraded to provide additional phase and intensity information of the manipulated thermal state for its use in quantum imaging applications [4,5]. Detailed experimental and theoretical exploration of such schemes is left for future work.

All relevant data are available from the Heriot-Watt University data archive [55].

ACKNOWLEDGMENTS

This work was supported by the UK Engineering and Physical Sciences Research Council (EPSRC) through the Quantum Communications Hub Grant No. EP/T001011/1 and Grant No. EP/N003446/1. G.T.’s studentship is funded by the EPSRC Grant No. EP/N509802/1 and the University of Strathclyde. For the purpose of open access, the author has

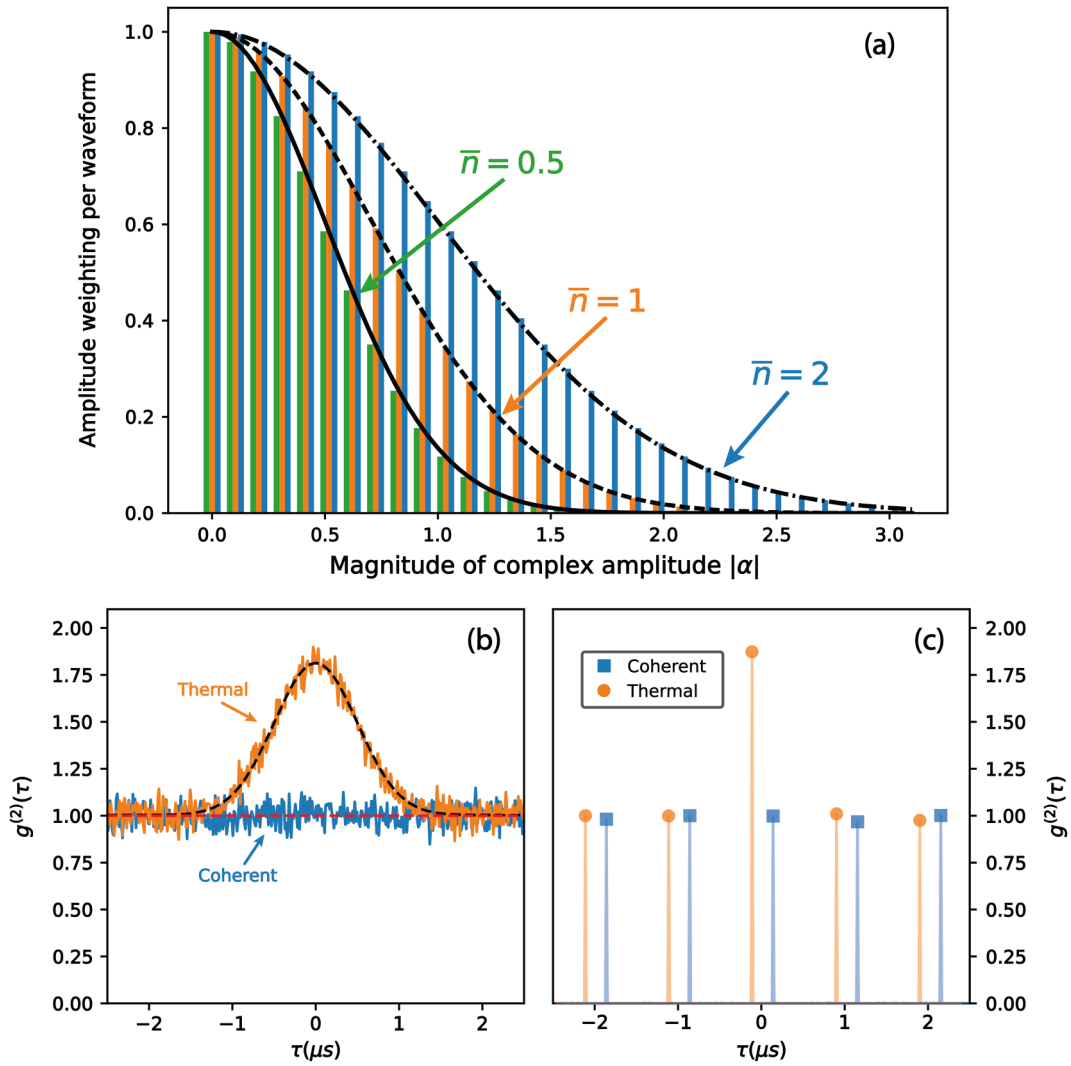


FIG. 7. (a) Relative weighting of each discretized amplitude for each thermal wave form. [(b), (c)] HBT second-order correlation measurements with $\bar{n} = 1.006$ for continuous-wave and pulsed mode respectively. Peaks in panel (c) have been artificially time-shifted to improve clarity.

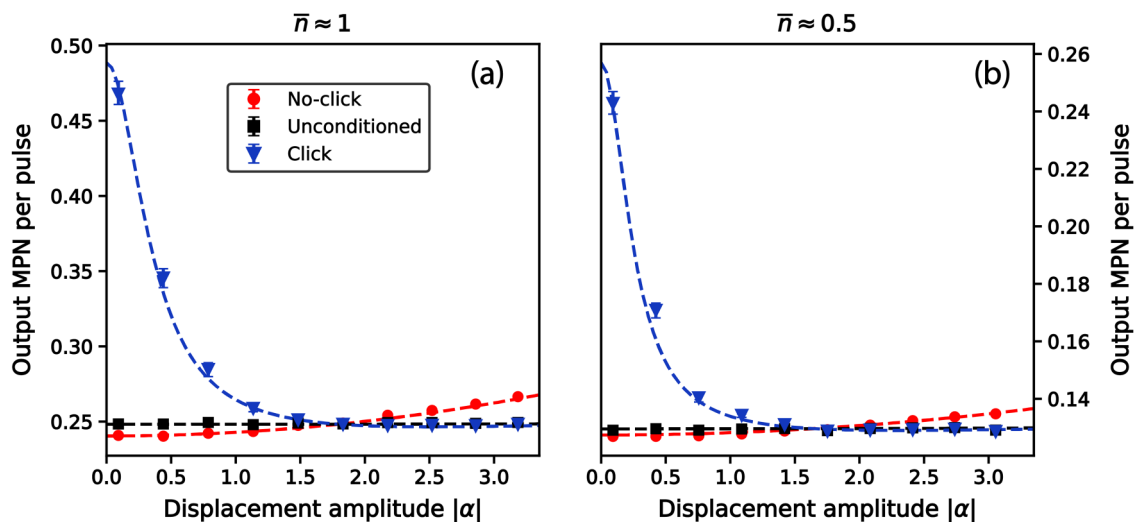


FIG. 8. Full range of experimentally measured values for (a) $\bar{n} \approx 1$ and (b) $\bar{n} \approx 0.5$.

applied a Creative Commons Attribution (CC BY) licence to any Author Accepted Manuscript version arising.

APPENDIX A: PHOTON SUBTRACTION OF DISPLACED THERMAL STATE - ALTERNATIVE METHOD

In the main text, we focus on the utility of the generalized two-mode moment-generating function (MGF) as it can be used to describe experimental implementations with arbitrary beam-splitter (BS) reflectance, as well as the limiting case of true photon subtraction. When one is only interested in true photon subtraction ($\beta = 0$, $r^2 \rightarrow 1$), we can derive the single-mode MGF of the displaced thermal state directly to be

$$M_{\text{th}}^{\alpha}(\mu) = \frac{1}{1 + \mu\bar{n}} \exp\left(-\frac{\mu|\alpha|^2}{1 + \mu\bar{n}}\right). \quad (\text{A1})$$

The utility of MGFs for photon subtraction is then apparent as photon subtraction leads to differentiation and renormalization of the MGF [39]

$$M_{\rho_{-1}}(\mu) = \frac{M'_{\rho}(\mu)}{M'_{\rho}(0)}. \quad (\text{A2})$$

Using Eqs. (A1) and (A2), one arrives at the same MGF for the photon-subtracted thermal state as in the main article and can proceed to obtain the mean photon number (MPN) as is done there.

APPENDIX B: OPTICAL SETUP AND DATA-ACQUISITION PROCEDURE

In order to verify experimentally the displaced-photon subtraction, we required a displaced thermal state, $\hat{\rho}_{\text{th}}^{-\alpha, \bar{n}}$, and a coherent state that could antidisplace it at an arbitrary ($t : r$) BS, $|(r/t)\alpha\rangle$. In order to do this, we used two adjacently coupled Mach-Zehnder interferometers (MZIs) as shown in Fig. 6, together with an outer tomography stage to perform state reconstruction and retrieve MPN information from the displaced thermal state. We derived a single-mode coherent input state from a fiber-coupled vertical cavity surface-emitting laser (VCSEL) diode of central wavelength of 848.2 nm (0.11 nm full width at half maximum linewidth) pulsed at 1 MHz repetition rate with 300 ps pulse width. The VCSEL was aligned with and coupled into the slow axis of a polarization-maintaining (PM) fiber. The rest of the experiment was performed using fiber-coupled PM components.

Throughout, the amplitude electro-optic modulator (EOM) is biased to minimize throughput at 0V. For each measurement point, the value of the displacement amplitude, $|\alpha|$, was set by varying l_b before intensity balancing the right hand *displaced photon subtraction* MZI at D_A , and the left-hand *state generation* MZI was intensity balanced at D_0 with the amplitude modulator set to maximum throughput via the RF voltage. The last MZI composing the tomography stage was intensity balanced by varying l_d while both maximizing the optical signal from BS₄ to BS₇ and minimizing the output of D_A . This configuration was achieved by blocking optical path l_b so that only the tuning signal from the EOMs was used for the balancing operation.

Once the interferometers had been intensity balanced, the EOMs were driven with paired 1 MHz pulse patterns from a

dual-output arbitrary waveform generator (AWG). The wave forms were generated in a cyclical pattern of five pulses: The first two pulses were used to tune the visibility at D_0 and the third and fourth pulses to tune the visibility at D_A (in such a way that the fourth pulse was producing destructive interference at that detector). The fourth pulse was also used to tune the cross visibility between detectors D_B and D_C (taking the output at D_C to be the one showing constructive interference) while the final fifth pulse was modulated with a pseudorandom amplitude-phase pair, $(|\alpha|^2, \phi)$ (chosen as described in the next section). Analyzing the final pulse of the cyclical pattern in postselection, our *displaced photon subtraction* (DPS) experiment was effectively running at the 200 kHz quoted in the main text. The active stabilization mechanism ensured that the relative phase differences between all optical paths were kept constant throughout the entire data acquisition process, allowing the system to achieve high interferometric visibilities, i.e., >90%, for the multiplexed reference signals. Only live-recorded measurements, integrated over a 1-s collection time, that exceeded a visibility threshold of $\approx 97\%$ were saved on a PC for off-line picosecond coincidence analysis via time-correlated single-photon counting techniques. The MPN of the reconstructed output state at the tomography stage was then calculated at D_B conditioned on either a click or no-click event from detector D_A .

The probability that a single-photon avalanche diode (SPAD) registers no-click when illuminated with a displaced thermal state is

$$P_{\chi} = \frac{1}{1 + \eta\bar{n}} \exp\left(-\frac{\eta|\alpha|^2}{1 + \eta\bar{n}}\right) \quad (\text{B1})$$

and the probability of a detection event is then $1 - P_{\chi}$. Thermal and coherent MPNs can then be calculated by setting the coherent and thermal MPN (respectively) to zero and correcting the measured count rates for experimental losses [33]. Experimental losses are the summation of nonunit detection efficiency, intrinsic component loss, as well as the use of a balanced beam splitter for the (ideally lossless) displacement operation. Given the structure of the interferometers, the MPN \bar{n} of the thermal state was found by systematically blocking the coherent component from optical paths l_b , l_c , and l_d and recording the count rates at detector D_B due only to the contribution from optical path l_a . Using Eq. (B1) and setting $|\alpha|^2$ to zero, a different value of \bar{n} could be extracted for different modulations from the electro-optic modulators. Similarly, the coherent displacement amplitude $|\alpha|$ was estimated by blocking optical paths l_a and l_c and measuring the count rates at detector D_0 from the contribution of optical path l_b via Eq. (B1).

APPENDIX C: P REPRESENTATION AND THERMAL STATE GENERATION

Coherent states form a nonorthogonal, $\langle\alpha|\beta\rangle = \exp(-\frac{1}{2}(|\alpha|^2 + |\beta|^2 - 2\alpha^*\beta))$, overcomplete basis. A state, $\hat{\rho}$ can be represented in this basis using the Glauber-Sudarshan P representation,

$$\hat{\rho} = \int P(\alpha)|\alpha\rangle\langle\alpha|d^2\alpha, \quad (\text{C1})$$

where $P(\alpha)$, the P function, is a quasiprobability distribution. For so-called *classical states* of light, the P function is a well-behaved probability distribution; thus, considering the complex amplitude in polar form, $\alpha = |\alpha| \exp i\phi$, any classical state can be approximated by modulating amplitude, $|\alpha|$, and phase, ϕ , according to the relevant P function, which is easily achieved using EOMs [30]. Using this method, we thermalized a coherent state source (red dashed box in Fig. 6) according to the Gaussian P function of a thermal state,

$$P(\alpha) = \frac{1}{\pi\bar{n}} \exp -\frac{|\alpha|^2}{\bar{n}}, \quad (\text{C2})$$

where $\bar{n} = \langle \hat{n} \rangle$ is the MPN of the thermal state [1]. All amplitudes (phases) are chosen from the range $|\alpha|^2 \in [0, 3]$ ($\phi \in [0, 2\pi]$) discretized into 50 evenly spaced values. For each data point, we generate a unique wave-form sampling the phase ϕ equiprobably, and the amplitude $|\alpha|$ weighted according to a discretized version of Eq. (C2). The relative weights for each MPN, $\bar{n} = 0.5, 1, \text{ and } 2$, used in this work

are shown in Fig. 7(a). We verified the thermal nature of the source by blocking all optical paths except the one connected to the EOMs (i.e., $l_b = l_c = l_d = 0$) and performing a Hanbury-Brown and Twiss (HBT) $g^{(2)}(0)$ correlation measurement between D_B and D_C , the results of which are shown in Figs. 7(b) and 7(c) for the case $\bar{n} = 1.006$ against those relative to a pure coherent source. Only the case $\bar{n} = 1.006$ is reported as all other \bar{n} cases showed similar results. Figures 7(b) and 7(c) show the HBT analysis of the modulated and unmodulated source for both continuous-wave and pulsed mode operation.

APPENDIX D: EXPLICIT DERIVATION OF TWO-MODE MOMENT GENERATING FUNCTION

The P function of a displaced thermal state, $\hat{\rho}_{\text{th}}^{(\bar{n}, \gamma)}$ is given by [1] $P(\alpha) = (1/\pi\bar{n}) \exp -|\alpha - \gamma|^2/\bar{n}$ and the input state after the beam-splitter transformation is given by

$$\begin{aligned} \hat{\rho}_{\text{out}} &= \hat{U}_{\text{BS}}^\dagger \hat{\rho}_{\text{th}}^{(\bar{n}, \gamma)} \hat{U}_{\text{BS}} = \frac{1}{\pi\bar{n}} \int e^{-\frac{|\alpha - \gamma|^2}{\bar{n}}} \delta^{(2)}(\beta_0 - \beta) \hat{U}_{\text{BS}}^\dagger |\alpha, \beta_0\rangle \langle \alpha, \beta_0| \hat{U}_{\text{BS}} d^2\alpha d^2\beta \\ &= \frac{1}{\pi\bar{n}} \int e^{-\frac{|\alpha - \gamma|^2}{\bar{n}}} |t\alpha - r\beta, t\beta + r\alpha\rangle \langle t\alpha - r\beta, t\beta + r\alpha| d^2\alpha \end{aligned} \quad (\text{D1})$$

The MGF associated with the state is then given by

$$\begin{aligned} M(\mu_1, \mu_2) &= \frac{1}{\pi\bar{n}} \int \exp -\frac{|\alpha - \gamma|^2}{\bar{n}} - \mu_1 |t\alpha - r\beta|^2 - \mu_2 |t\beta + r\alpha|^2 d^2\alpha \\ &= \frac{1}{1 + \mu_1 t^2 \bar{n} + \mu_2 r^2 \bar{n}} \exp -\frac{\mu_1 |t\gamma - r\beta|^2 + \mu_2 |r\gamma + t\beta|^2 + |\beta|^2 \bar{n} \mu_1 \mu_2}{1 + t^2 \mu_1 \bar{n} + r^2 \mu_2 \bar{n}}. \end{aligned} \quad (\text{D2})$$

Note that in the main text the displacement amplitude is α instead of γ that appears here.

APPENDIX E: P FUNCTION OF THE OUTPUT STATE

The P function of the output state after the DPS is a difference of Gaussian functions and therefore non-Gaussian. The output state, in the P representation, is given by

$$\hat{\rho} = \frac{1}{\pi\bar{n}r^2 P_{\mathcal{C}}} \int \exp -\frac{|\gamma - t\beta - r\alpha|^2}{r^2 \bar{n}} - \exp -\frac{(1 + \eta\bar{n}t^2)}{\bar{n}r^2} \left| \gamma - t\beta - \frac{r(\alpha + \eta t r \bar{n} \beta)}{1 + \eta\bar{n}t^2} \right|^2 - \frac{\eta}{1 + \eta\bar{n}t^2} |t\alpha - r\beta|^2 |\gamma\rangle \langle \gamma| d^2\gamma. \quad (\text{E1})$$

-
- [1] C. Gerry, P. Knight, and P. L. Knight, *Introductory Quantum Optics* (Cambridge University Press, Cambridge, UK, 2005)
- [2] R. Hanbury-Brown and R. Q. Twiss, Correlation between photons in two coherent beams of light, *Nature (London)* **177**, 27 (1956).
- [3] A. Gatti, E. Brambilla, M. Bache, and L. A. Lugiato, Ghost Imaging with Thermal Light: Comparing Entanglement and Classical Correlation, *Phys. Rev. Lett.* **93**, 093602 (2004).
- [4] F. Ferri, D. Magatti, A. Gatti, M. Bache, E. Brambilla, and L. A. Lugiato, High-Resolution Ghost Image and Ghost Diffraction Experiments with Thermal Light, *Phys. Rev. Lett.* **94**, 183602 (2005).
- [5] A. Valencia, G. Scarcelli, M. D'Angelo, and Y. Shih, Two-Photon Imaging with Thermal Light, *Phys. Rev. Lett.* **94**, 063601 (2005).
- [6] S. Lloyd, Enhanced sensitivity of photodetection via quantum illumination, *Science* **321**, 1463 (2008).
- [7] I. A. Fedorov, A. E. Ulanov, Y. V. Kurochkin, and A. I. Lvovsky, Quantum vampire: Collapse-free action at a distance by the photon annihilation operator, *Optica* **2**, 112 (2015).
- [8] K. G. Katamadze, G. V. Avosopiants, Y. I. Bogdanov, and S. P. Kulik, How quantum is the “quantum vampire” effect? Testing with thermal light, *Optica* **5**, 723 (2018).
- [9] A. Zavatta, V. Parigi, M. S. Kim, H. Jeong, and M. Bellini, Experimental Demonstration of the Bosonic Commutation Relation Via Superpositions of Quantum Operations on Thermal Light Fields, *Phys. Rev. Lett.* **103**, 140406 (2009).
- [10] V. Parigi, A. Zavatta, M. Kim, and M. Bellini, Probing quantum commutation rules by addition and subtraction of single photons to/from a light field, *Science* **317**, 1890 (2007).

- [11] M. D. Vidrighin, O. Dahlsten, M. Barbieri, M. S. Kim, V. Vedral, and I. A. Walmsley, Photonic Maxwell's Demon, *Phys. Rev. Lett.* **116**, 050401 (2016).
- [12] S. Wang, L. Y. Hu, and H. Y. Fan, Nonclassical properties of multiple-photon subtracted displaced squeezed thermal states, *Eur. Phys. J. D* **66**, 166 (2012).
- [13] A. Allevi, A. Andreoni, M. Bondani, M. G. Genoni, and S. Olivares, Reliable source of conditional states from single-mode pulsed thermal fields by multiple-photon subtraction, *Phys. Rev. A* **82**, 013816 (2010).
- [14] A. R. Usha Devi, R. Prabhu, and M. S. Uma, Non-classicality of photon added coherent and thermal radiations, *Eur. Phys. J. D* **40**, 133 (2006).
- [15] S. M. H. Rafsanjani, M. Mirhosseini, O. S. M. na Loaiza, B. T. Gard, R. Birrittella, B. E. Koltenebah, C. G. Parazzoli, B. A. Capron, C. C. Gerry, J. P. Dowling, and R. W. Boyd, Quantum-enhanced interferometry with weak thermal light, *Optica* **4**, 487 (2017).
- [16] F. S. Roux, Toolbox for non-classical state calculations, *J. Opt.* **23**, 125201 (2021).
- [17] G. V. Avosopiants, B. I. Bantysh, K. G. Katamadze, N. A. Bogdanova, Y. I. Bogdanov, and S. P. Kulik, Statistical parameter estimation of multimode multiphoton-subtracted thermal states of light, *Phys. Rev. A* **104**, 013710 (2021).
- [18] K. G. Katamadze, G. V. Avosopiants, N. A. Bogdanova, Y. I. Bogdanov, and S. P. Kulik, Multimode thermal states with multiphoton subtraction: Study of the photon-number distribution in the selected subsystem, *Phys. Rev. A* **101**, 013811 (2020).
- [19] C. Kumar, J. Singh, S. Bose, and Arvind, Coherence-assisted non-Gaussian measurement-device-independent quantum key distribution, *Phys. Rev. A* **100**, 052329 (2019).
- [20] C. N. Gagatsos and S. Guha, Efficient representation of Gaussian states for multimode non-Gaussian quantum state engineering via subtraction of arbitrary number of photons, *Phys. Rev. A* **99**, 053816 (2019).
- [21] S. Olivares, A. Allevi, and M. Bondani, Gaussian and non-Gaussian operations on non-Gaussian state: Engineering non-Gaussianity, *Quantum Meas. Quantum Metrol.* **2**, 0001 (2014).
- [22] J. Sperling, W. Vogel, and G. S. Agarwal, Quantum state engineering by click counting, *Phys. Rev. A* **89**, 043829 (2014).
- [23] I. D. Ivanovic, How to differentiate between non-orthogonal states, *Phys. Lett. A* **123**, 257 (1987).
- [24] B. Huttner, N. Imoto, N. Gisin, and T. Mor, Quantum cryptography with coherent states, *Phys. Rev. A* **51**, 1863 (1995).
- [25] W. Yu, Z. Xiong, Z. Dong, Y. Xu, W. Liu, Z. Qu, and A. X. Liu, The numerical results of binary coherent-state signal's quantum detection in the presence of noise, in *Artificial Intelligence and Security*, edited by X. Sun, J. Wang, and E. Bertino (Springer International, Berlin, 2020), pp. 532–542
- [26] R. Filip, Continuous-variable quantum key distribution with noisy coherent states, *Phys. Rev. A* **77**, 022310 (2008).
- [27] Z. Yang, X. Guan, B. Luo, L. Yin, G. Gao, and J. Chen, Ambient light suppressed free space optical communication system based on FADOF, in *2019 18th International Conference on Optical Communications and Networks (ICOON)* (IEEE, Huangshan, China, 2019), pp. 1–3.
- [28] K. Blow and D. Wood, Theoretical description of transient stimulated Raman scattering in optical fibers, *IEEE J. Quantum Electron.* **25**, 2665 (1989).
- [29] P. Marek and R. Filip, Coherent-state phase concentration by quantum probabilistic amplification, *Phys. Rev. A* **81**, 022302 (2010).
- [30] M. A. Usuga, C. R. Müller, C. Wittmann, P. Marek, R. Filip, C. Marquardt, G. Leuchs, and U. L. Andersen, Noise-powered probabilistic concentration of phase information, *Nat. Phys.* **6**, 767 (2010).
- [31] E. Eleftheriadou, S. M. Barnett, and J. Jeffers, Quantum Optical State Comparison Amplifier, *Phys. Rev. Lett.* **111**, 213601 (2013).
- [32] R. J. Donaldson, R. J. Collins, E. Eleftheriadou, S. M. Barnett, J. Jeffers, and G. S. Buller, Experimental Implementation of a Quantum Optical State Comparison Amplifier, *Phys. Rev. Lett.* **114**, 120505 (2015).
- [33] R. Donaldson, L. Mazzarella, R. Collins, J. Jeffers, and G. S. Buller, A high-gain and high-fidelity coherent state comparison amplifier, *Commun. Phys.* **1**, 54 (2018).
- [34] D. W. Canning, R. J. Donaldson, S. Mukherjee, R. J. Collins, L. Mazzarella, U. Zanforlin, J. Jeffers, R. R. Thomson, and G. S. Buller, On-chip implementation of the probabilistic quantum optical state comparison amplifier, *Opt. Express* **27**, 31713 (2019).
- [35] M. S. Kim, E. Park, P. L. Knight, and H. Jeong, Nonclassicality of a photon-subtracted Gaussian field, *Phys. Rev. A* **71**, 043805 (2005).
- [36] A. Ourjoumtsev, R. Tualle-Brouiri, J. Laurat, and P. Grangier, Generating optical Schrödinger kittens for quantum information processing, *Science* **312**, 83 (2006).
- [37] P. Marek, J. Provazník, and R. Filip, Loop-based subtraction of a single photon from a traveling beam of light, *Opt. Express* **26**, 29837 (2018).
- [38] Y. Kurochkin, A. S. Prasad, and A. I. Lvovsky, Distillation of the Two-Mode Squeezed State, *Phys. Rev. Lett.* **112**, 070402 (2014).
- [39] Y. I. Bogdanov, K. G. Katamadze, G. V. Avosopiants, L. V. Belinsky, N. A. Bogdanova, A. A. Kalinkin, and S. P. Kulik, Multiphoton subtracted thermal states: Description, preparation, and reconstruction, *Phys. Rev. A* **96**, 063803 (2017).
- [40] S. M. Barnett, G. Ferenczi, C. R. Gilson, and F. C. Speirits, Statistics of photon-subtracted and photon-added states, *Phys. Rev. A* **98**, 013809 (2018).
- [41] P. Kelley and W. Kleiner, Theory of electromagnetic field measurement + photoelectron counting, *Phys. Rev.* **136**, A316 (1964).
- [42] Since we have that $\hat{\rho}|_{\mathcal{X}} = \text{Tr}_2[\hat{\rho}_{1,2} : e^{-\eta\hat{a}_2^\dagger\hat{a}_2} :]/\text{Tr}_{1,2}[\hat{\rho}_{1,2} : e^{-\eta\hat{a}_2^\dagger\hat{a}_2} :]$.
- [43] R. J. Glauber, Coherent and incoherent states of the radiation field, *Phys. Rev.* **131**, 2766 (1963).
- [44] E. C. G. Sudarshan, Equivalence of Semiclassical and Quantum Mechanical Descriptions of Statistical Light Beams, *Phys. Rev. Lett.* **10**, 277 (1963).
- [45] G. S. Buller and R. J. Collins, Single-photon generation and detection, *Meas. Sci. Technol.* **21**, 012002 (2010).
- [46] F. T. Arecchi, Measurement of the Statistical Distribution of Gaussian and Laser Sources, *Phys. Rev. Lett.* **15**, 912 (1965).
- [47] U. Zanforlin, R. J. Donaldson, R. J. Collins, and G. S. Buller, Analysis of the effects of imperfections in an optical heterodyne quantum random-number generator, *Phys. Rev. A* **99**, 052305 (2019).

- [48] F. Flamini, L. Magrini, A. S. Rab, N. Spagnolo, V. D'Ambrosio, P. Mataloni, F. Sciarrino, T. Zandrini, A. Crespi, R. Ramponi, and R. Osellame, Thermally reconfigurable quantum photonic circuits at telecom wavelength by femtosecond laser micromachining, *Light Sci. Appl.* **4**, e354 (2015).
- [49] R. J. Donaldson, L. Mazzarella, U. Zanforlin, R. J. Collins, J. Jeffers, and G. S. Buller, Quantum state correction using a measurement-based feedforward mechanism, *Phys. Rev. A* **100**, 023840 (2019).
- [50] L. Mazzarella, R. J. Donaldson, R. J. Collins, U. Zanforlin, G. Tatti, G. S. Buller, and J. Jeffers, Quantum state comparison amplifier with feedforward state correction, in *Quantum Technologies 2018*, Vol. 10674, edited by J. Stuhler, A. J. Shields, and M. J. Padgett (International Society for Optics and Photonics, Strasbourg, France, 2018), pp. 153–161.
- [51] M. Curty, X. Ma, B. Qi, and T. Moroder, Passive decoy-state quantum key distribution with practical light sources, *Phys. Rev. A* **81**, 022310 (2010).
- [52] B. Qi, P. G. Evans, and W. P. Grice, Passive state preparation in the Gaussian-modulated coherent-states quantum key distribution, *Phys. Rev. A* **97**, 012317 (2018).
- [53] E. Newton, A. Ghesquière, F. L. Wilson, B. T. H. Varcoe, and M. Moseley, Quantum secrecy in thermal states, *J. Phys. B: At. Mol. Opt. Phys.* **52**, 125501 (2019).
- [54] E. Newton, A. Ghesquière, F. L. Wilson, R. F. Guiazon, B. T. H. Varcoe, and M. Moseley, Quantum secrecy in thermal states II, *J. Phys. B: At. Mol. Opt. Phys.* **53**, 205502 (2020).
- [55] G. Tatti, D. W. Canning, U. Zanforlin, L. Mazzarella, J. Jeffers, and G. S. Buller, Dataset for "Manipulating thermal light via displaced-photon subtraction", Heriot-Watt University (2022), doi: 10.17861/57cbd041-e6e3-4c77-96a5-04077ddd1111.